

Generation of integer and fractional perfect vortex beams using all-dielectric geometrical phase metasurfaces

Cite as: Appl. Phys. Lett. **120**, 201701 (2022); <https://doi.org/10.1063/5.0094549>

Submitted: 04 April 2022 • Accepted: 10 May 2022 • Published Online: 18 May 2022

Kaixiang Cheng, Zexu Liu, Zheng-Da Hu, et al.



View Online



Export Citation



CrossMark

ARTICLES YOU MAY BE INTERESTED IN

[Vector beam generation based on spin-decoupling metasurface zone plate](#)

Applied Physics Letters **120**, 191704 (2022); <https://doi.org/10.1063/5.0093708>

[Broadband spin-unlocked metasurfaces for bifunctional wavefront manipulations](#)

Applied Physics Letters **120**, 181702 (2022); <https://doi.org/10.1063/5.0091051>

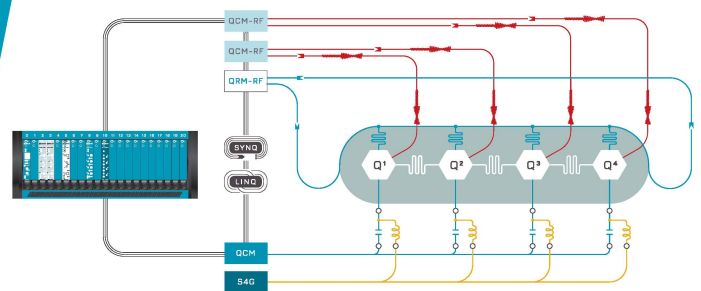
[Inverse design of Pancharatnam–Berry phase metasurfaces for all-optical image edge detection](#)

Applied Physics Letters **120**, 241101 (2022); <https://doi.org/10.1063/5.0090606>

 QBLOX

Integrates all
Instrumentation + Software
for Control and Readout of
Superconducting Qubits

[visit our website >](#)



Generation of integer and fractional perfect vortex beams using all-dielectric geometrical phase metasurfaces

Cite as: Appl. Phys. Lett. **120**, 201701 (2022); doi: 10.1063/5.0094549

Submitted: 4 April 2022 · Accepted: 10 May 2022 ·

Published Online: 18 May 2022 · Publisher error corrected: 31 May 2022



View Online



Export Citation



CrossMark

Kaixiang Cheng,¹ Zexu Liu,¹ Zheng-Da Hu,¹ Guoyang Cao,¹ Jingjing Wu,¹ and Jicheng Wang^{1,2,a)} 

AFFILIATIONS

¹School of Science, Jiangsu Provincial Research Center of Light Industrial Optoelectronic Engineering and Technology, Jiangnan University, Wuxi 214122, China

²State Key Laboratory of Applied Optics, Changchun Institute of Optics, Fine Mechanics and Physics, Chinese Academy of Sciences, Changchun 130033, China

^{a)}Author to whom correspondence should be addressed: jcwang@jiangnan.edu.cn

ABSTRACT

Perfect vortex (PV) beams possess a radial intensity profile independent of their topological charges, overcoming the defects of the regular vortex beams. However, the bulky optical elements used in conventional methods for generation of PV beams limit their potential applications. Metasurfaces are ultra-thin version of metamaterials with the flexible ability of controlling electromagnetic waves, promising great potential applications in many optical fields. Here, an all-dielectric metasurface based on a geometrical phase is demonstrated, featuring broadband and high efficiency in manipulation of circularly polarized light. We numerically simulate the performance of the unit-cell and metasurface for generating PV beams carrying integer and fractional topological charges. We hope the designed metasurface will provide an ultra-compact way for generation of high-quality PV beams.

Published under an exclusive license by AIP Publishing. <https://doi.org/10.1063/5.0094549>

A vortex beam is a special type of light beam with a helical phase profile and a rotating wave front along the optical axis. It can be quantitatively defined by the phase factor $e^{il\theta}$, where l and θ denote the topological charge and azimuthal angle, respectively. As a result, a vortex beam has the ability of carrying orbital angular momentum $l\hbar$ per photon with a doughnut-shaped intensity profile.^{1,2} Due to these unique features, vortex beams have been adopted for various kinds of applications, such as optical communication,³ optical manipulation,⁴ and quantum information processing.⁵ However, the diameter of the annular intensity profile of vortex beams is highly related to their topological charges, which greatly limit their applications. To overcome this problem, Ostrovsky *et al.* introduced a novel concept of a “perfect” vortex (PV) beam, which has constant intensity profile with the diameter independent of the topological charge.⁶ In order to obtain PVs, many schemes have been reported, such as using axicons,⁷ spatial light modulators,⁸ or a combination of the two.⁹ However, these methods all require bulky optical elements, increasing the complexity and hindering the application of PV beams in multi-element photonic systems.

Metasurfaces, which are two-dimensional version of metamaterials, have been widely studied. Benefiting from their ultra-thin profiles

and the ability to flexibly manipulate amplitudes, phases, and polarization states of incident electromagnetic waves at a subwavelength scale,¹⁰ metasurfaces have great potential for many optical applications, such as meta-lens,¹¹ holograms,¹² vortex beams,^{13–15} and vector beams.¹⁶ These devices may pave the way for microscopy¹⁴ or optical encryption with high-efficiency and compact features.¹⁵ Metasurfaces have also been used for generating PV beams.^{17–23} However, some of these methods faced with restricted efficiencies caused by metal loss^{17,18} or simultaneous phase and amplitude modulation in the design process.¹⁹ The pure phase method based on phase superposition with relatively high efficiency is then applicable for PV beams generation.^{20–23} Usage of a propagation phase²⁰ may bring problem of selecting unit-cells with different dimensions. The method demonstrated in Refs. 21–23 based on the geometrical phase has solved this problem, obtaining high-quality PV beams at the visible and ultraviolet band. Nevertheless, all these works mentioned above just discussed the generation of PV beams with integer topological charges. Fractional vortex beams with fractional topological charges rather than integer ones, possessing unique low-intensity gaps on their intensity profile, have attracted increasing attention.²⁴ In the field of optical

manipulation, their unique properties can be used in some novel applications like cell sorting and precise control of cell orientation.^{25,26} They can also expand the communication capacity in optical communication systems.²⁷

In this Letter, we demonstrate the efficiency up to 80% and broadband generation of PV beams using dielectric silicon metasurfaces with the geometrical phase in the near-infrared band. We design and simulate metasurfaces generating PV beams with integer and fractional topological charges with circular ring and ellipse ring intensity profiles. Our work provides a potential compact scheme with high efficiency and wide operation bandwidth, which can be utilized for many applications like high-capacity optical communication and optical manipulation.

It has been proved that a PV beam can be generated by the Fourier transform of a Bessel beam,²⁸ and in practice, a Bessel–Gaussian beam generated by an axicon is used because the realization of an ideal Bessel beam is not possible. Then the electric field at the rear focal plane of the Fourier lens (i.e., the Fourier transform of the incident Bessel–Gaussian beam) can be written as²⁸

$$E(r, \theta) = i^{l-1} \frac{w_g}{w_0} \exp(il\theta) \exp\left(-\frac{r^2 + R^2}{w_0^2}\right) I_l\left(\frac{2Rr}{w_0^2}\right), \quad (1)$$

where w_g is the waist of the incident Gaussian beam, w_0 is the Gaussian beam waist at the focus. R is the ring radius of the PV beam and equals to $k_r f / k$, where k_r is the radial wavevector [related to the numerical aperture (NA) of the axicon], and f is the focal length of the lens. I_l is the modified Bessel function of the first kind. From Eq. (1), we can find that the intensity profile of the PV beam is shaped by the Gaussian function and the modified Bessel function. This result indicates that a Gaussian beam passing through an axicon, a spiral phase plate, and a Fourier lens can generate a PV beam carrying topological charge matches with the topological charge according to the spiral phase plate, and its profile can be controlled by changing the parameters of the axicon. Here, we realize all these functions of these elements mentioned above by combining their phase profiles via a metasurface [shown in Fig. 1(a)]. The phase distribution φ_{meta} on the metasurface can be expressed as

$$\varphi_{\text{meta}} = \varphi_{\text{spiral}} + \varphi_{\text{axicon}} + \varphi_{\text{lens}}, \quad (2)$$

$$\varphi_{\text{spiral}} = l \arctan\left(\frac{ey}{x}\right), \quad (3)$$

$$\varphi_{\text{axicon}} = -\frac{2\pi NA}{\lambda} \sqrt{x^2 + e^2 y^2}, \quad (4)$$

$$\varphi_{\text{lens}} = -\pi \frac{x^2 + y^2}{\lambda f}, \quad (5)$$

where l is the topological charge of the vortex beam, e defines the ellipticity of the PV beam, and λ is the working wavelength of the lens. Figure 1(b) shows the schematic diagram of the designed metasurface with the phase profile defined above. The unit-cell of the metasurface is rectangular c-silicon nanopillar with height $H = 600$ nm and in-plane dimensions D_x and D_y , arranged on the sapphire substrate. The period P of the unit-cell is 400 nm. Due to the fact that c-silicon has low loss and high refractive index at the infrared band, we choose it as a building block of the metasurface. For metasurface processing the geometrical phase [or Pancharatnam–Berry (PB) phase], the unit-cell, with similar function of the half-wave plate, can yield a 2θ phase shift of the incident circularly polarized wave, where θ represents the rotation angle of the nanopillar. Thus, the unit-cell can realize a full 2π phase shift continuously by changing its rotation angle.

Because the metasurface based on the geometrical phase can convert the circularly polarized wave into the cross-polarized wave and only add the additional phase shift on the cross-polarized component, we need to optimize the geometrical parameters of the nanopillar to maximize the cross-polarized component. The polarization conversion efficiency (PCE) is defined as the proportion of the cross-polarized component in the total transmitted wave. Figure 2(a) shows the simulated PCE vs nanopillar geometrical parameters D_x and D_y , at 780 nm near-infrared incidence. The simulation is implemented using the finite-difference time-domain (FDTD) method based on the periodic boundary condition. Based on the simulated result, we set D_x and D_y as 186 and 122 nm, respectively, to obtain the highest PCE [red point in Fig. 2(a)]. As shown in Fig. 2(b), the nanopillar behaves as a half-wave plate and exhibits a nearly π phase retardance between the p - and s -polarized incidence. In order to study the broadband

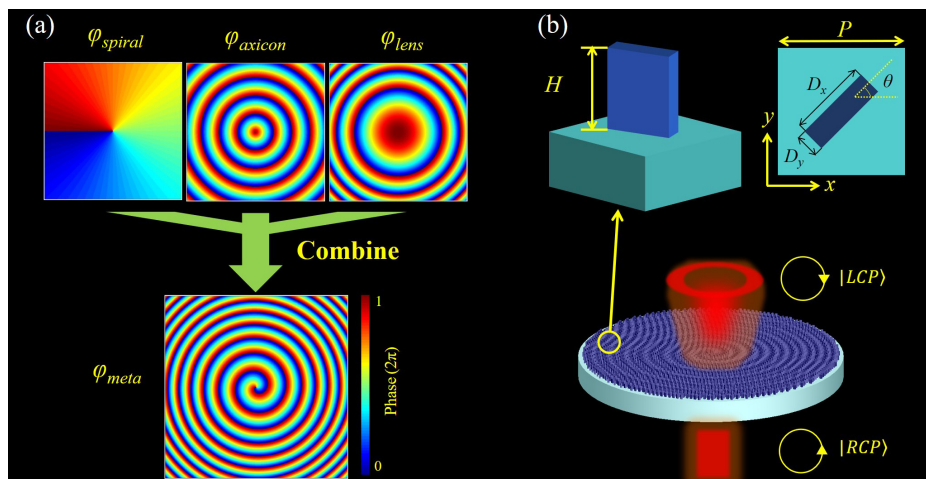


FIG. 1. (a) Generation of the phase profile of the designed metasurface by superposition of three phase profiles of the spiral phase plate, axicon, and focusing lens. (b) Schematic diagram of the designed metasurface and the unit-cell. The metasurface can convert the right-hand circularly polarized light (RCP) into left-hand circularly polarized light (LCP) with designed phase shift, that is, convert the incident RCP Gaussian beam into the LCP PV beam.

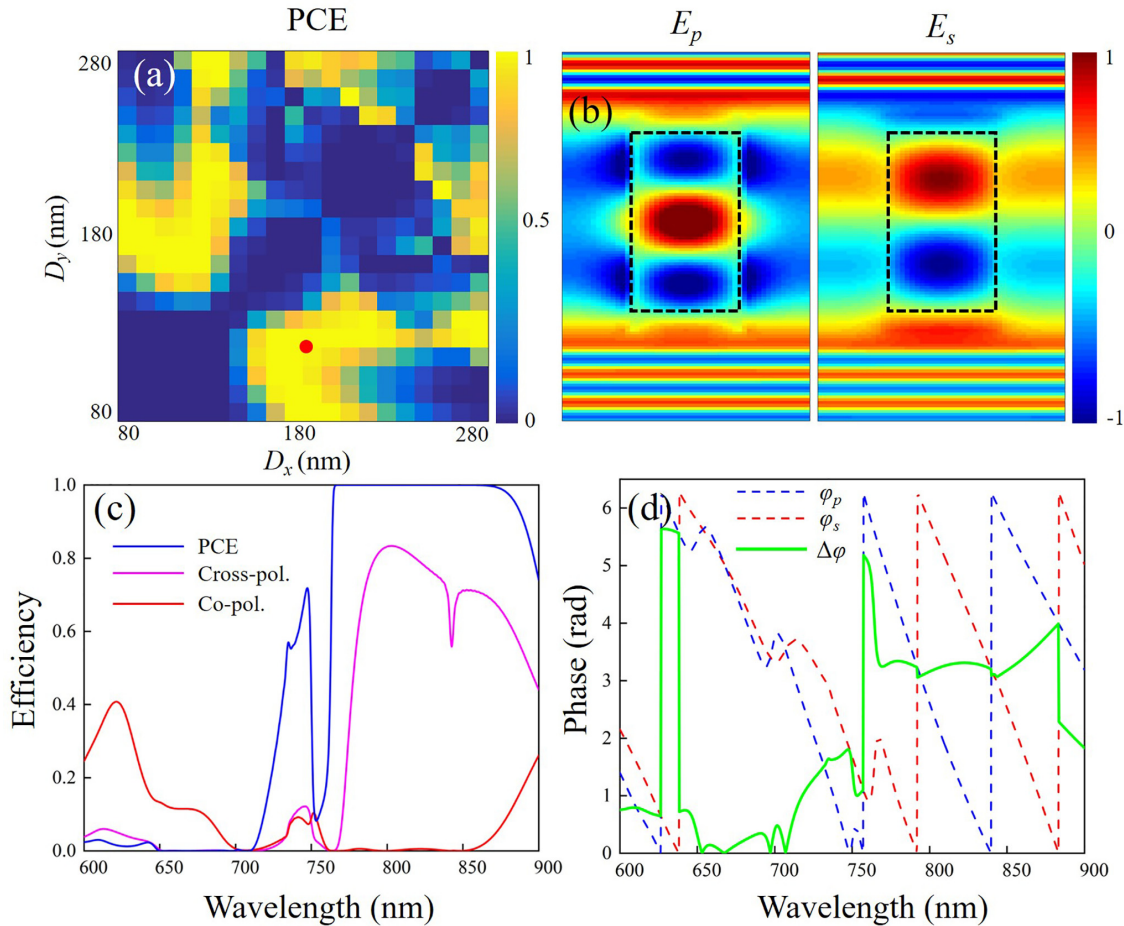


FIG. 2. (a) Simulated PCE vs nanopillar geometrical parameters D_x and D_y at 780 nm near-infrared incidence. The red point represents the selected dimensions of the unit-cell. (b) Simulated normalized electric field distribution of the p - and s -polarized incidence, respectively, which shows the phase retardance between p - and s -polarized waves. The black dashed rectangles represent the region of the nanopillar. (c) Simulated efficiency of co-, cross-polarized transmitted wave and PCE at the 600–900 nm band. (d) Simulated phase shift between p - and s -polarized incidence and the transmitted wave, and the phase difference between the p - and s -polarized incidence.

performance of the designed unit-cell, we calculate the PCE and phase retardance between the p - and s -polarized waves of the unit-cell with the geometrical parameters determined within a range of 600–900 nm incidence. The results are shown in Figs. 2(c) and 2(d). From the simulated results, we can find that the transmittance of the cross-polarized component is above 50% and PCE maintains above 80% at the 730–880 nm band, and the phase retardance between the p - and s -polarized incidence maintains close to π . Due to the fact that unit-cells of the geometrical phase-based metasurface have the same dimensions and only the rotation angle differs, these results reveal the potential high performance of the designed metasurface based on this unit-cell at the 730–880 nm band.

According to the discussion of the unit-cell properties above, the silicon nanopillars with selected size are used for arranging the whole metasurface. By controlling the rotation angle θ of each unit-cell, we can map the phase profile φ_{meta} for generating a PV beam to the physical structure of the metasurface ($\theta = \varphi_{\text{meta}}/2$ according to the geometrical phase). Next, we perform numerical simulation [the FDTD method

based on perfectly matched layer (PML) boundary conditions at all dimensions] to test the potential performance of the designed metasurface. We first design three metasurfaces for generating PV beams with topological charge $l = 1, 2, \text{ and } 3$, respectively. Here, the ellipticity e of the PV beam is set to 1 (i.e., a PV beam with a circular ring intensity profile), the NA of axicon is 0.2, and the focal length of the lens is $15 \mu\text{m}$. First, we use circularly polarized Gaussian beam incidence with 780 nm wavelength for testing the single wavelength point performance of the metasurface. For balancing the result accuracy and computational load, we use a metasurface array consisting of 2828 unit-cells in the simulation. Figures 3(a)–3(c) show the simulated intensity profile of the generated PV beams at the focal plane with topological charges $l = 1, 2, \text{ and } 3$, respectively. We can find that the sizes of the PV beams are nearly the same, and the diameters of the PV beams with topological charge $l = 1, 2, \text{ and } 3$ are 7.5, 7.8, and $8.3 \mu\text{m}$, respectively. The difference is mainly caused by the down sampling of the continuous phase profile in the numerical simulation and can be further improved in experiments by increasing the quantity of the unit-cells. Figures

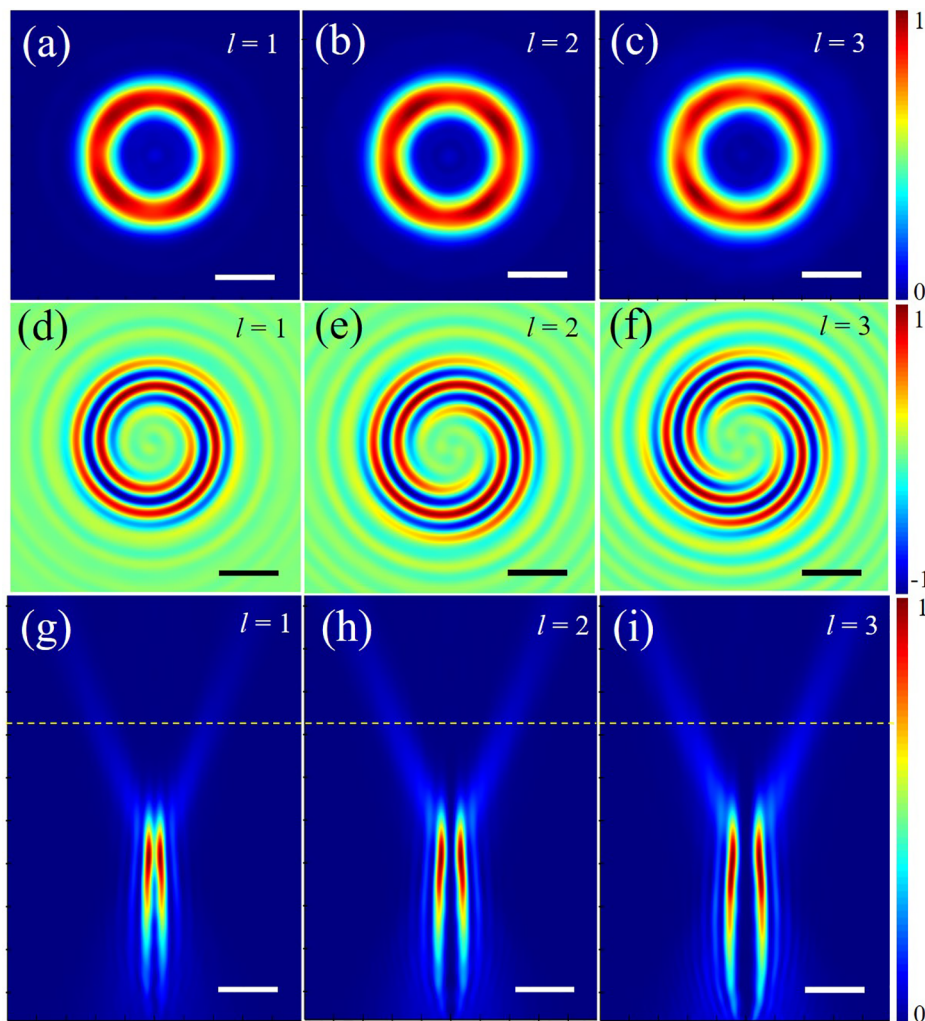


FIG. 3. Simulated results of metasurfaces for generating PV beams with different topological charges. (a)–(c) Normalized intensity profile at the focal plane for PV beams with $l = 1, 2,$ and 3 . (d)–(f) Normalized real part of the electric field at the focal plane for PV beams with $l = 1, 2,$ and 3 . (g)–(i) Normalized intensity profile at the x - z plane for PV beams with $l = 1, 2,$ and 3 . The yellow dashed line represents the focal length ($15 \mu\text{m}$). Scale bar: $4 \mu\text{m}$.

3(d)–3(f) show the real parts of the electric fields of generated PV beams at the focal plane, which indicate the different topological charges of the generated PV beams, and they are equivalent to the designed topological charges. The intensity distributions in the x - z plane are shown in Figs. 3(g)–3(i). Here, we can observe the evolution of the Gaussian beams after transmitted from the metasurface. The Gaussian beam is first converted into the Bessel-like hollow beam carrying certain topological charge with low divergence angle away from the focal plane and then converted into the diverging doughnut-shaped hollow beam near the focal plane and propagating with a fixed profile after the focal plane. We can find that the intensity profile behind the focal plane is irrelevant to the topological charge, indicating the generation of the PV beam. The simulated generation efficiencies (defined by the power ratio of the generated cross-polarized PV beams at the focal plane and the incident beam) of the metasurfaces generating PVs with $l = 1, 2,$ and 3 , are 80.0%, 77.7%, and 76.3%, respectively.

To explore the broadband performance of the designed metasurface, we use the incident circularly polarized Gaussian beam at other three different wavelengths, 730, 830, and 880 nm, to simulate the

output of the metasurface. The topological charge l is set as 1 in these simulations. Figures 4(a)–4(c) show the simulated intensity profile at the focal plane. Note that although the metasurface features broadband property, the focal length still varies with the incident wavelength due to the dispersion according to Eq. (5), so the intensity profiles in Figs. 4(a)–4(c) are collected at $z = 16, 14,$ and $13 \mu\text{m}$. The diameters of the PV beams for 730, 830, and 880 nm incidence are 8.1, 8, and $8.2 \mu\text{m}$, respectively. The simulated generation efficiencies of the metasurface are 27.5% at 730 nm, 76.9% at 830 nm, and 58.2% at 880 nm. Note that the simulated efficiency of the whole metasurface is lower than the results of unit-cells simulation mentioned above. The difference is mainly caused by the near-field coupling of adjacent nanopillars with different orientations. Due to the simulation of the unit-cell based on periodic boundary condition, which assumes a uniform array and without this problem, the simulated efficiency of the unit-cell is higher than the whole metasurface.

To generate an elliptical PV beam, we set ellipticity e as 0.7 and use 830 nm incidence in the simulation. Figures 4(d)–4(f) show the simulated intensity profile of the elliptical PV beams at the focal plane

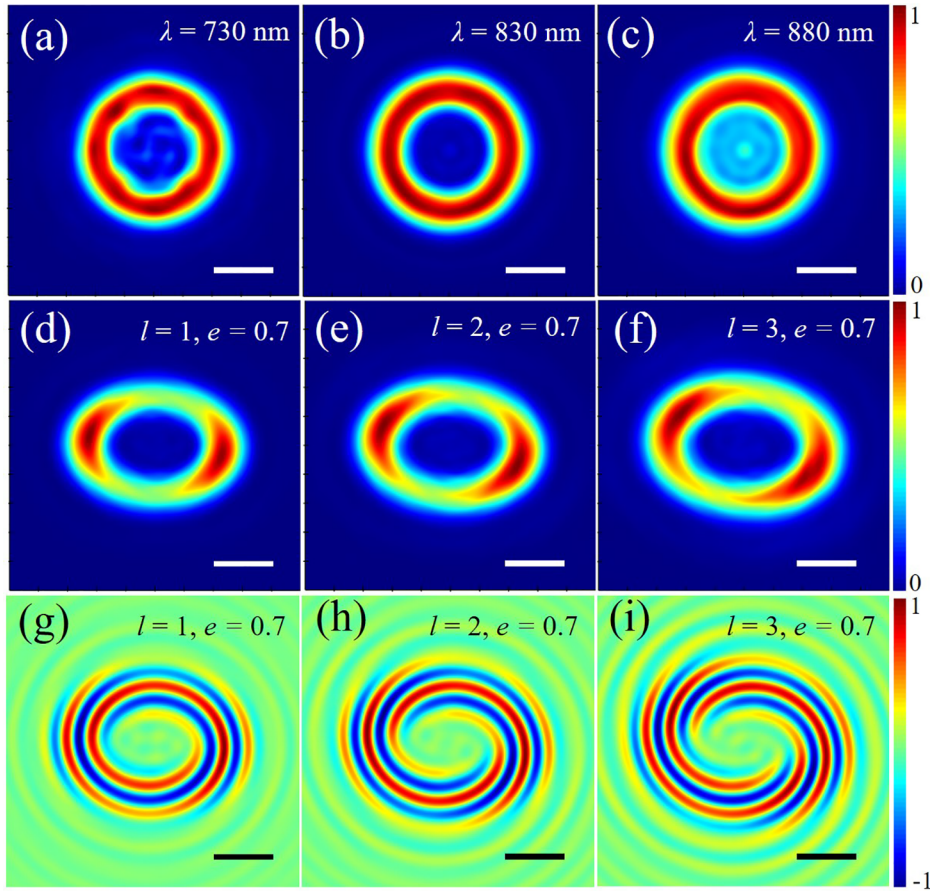


FIG. 4. (a)–(c) Simulated intensity profile at 730, 830, and 880 nm, respectively; here, the topological charge l is set as 1. (d)–(f) Simulated intensity profile of elliptical PVs with different l , ellipticity $e = 0.7$. (g)–(i) Simulated real part of the electric field corresponding to (d)–(f). Scale bar: $4 \mu\text{m}$.

($z = 14 \mu\text{m}$) with $l = 1, 2$, and 3 . Figures 4(g)–4(i) show the simulated real parts of the electric fields at the focal plane, which indicate the different topological charges of the elliptical PV beams. The simulated ellipticities of the elliptical PVs are 0.67, 0.69, and 0.71, which match well with our design. The simulated generation efficiencies are 77.2%, 76.2%, and 74.6% for elliptical PV beams with $l = 1, 2$, and 3 .

Next, we simulate the metasurface for generation of fractional elliptical PVs. The ellipticity e is set as 1.1. Figure 5(a) shows the spiral phase patterns [φ_{spiral} in Eq. (3)] of the fraction vortex with $l = 0.5$ and $l = 1.5$ in Figs. 5(b) and 5(c). Figures 5(d)–5(f) show the theoretical calculated far-field intensity profile corresponding to the conditions in Figs. 5(a)–5(c) using the scalar diffraction theory, and Figs. 5(g)–5(i) show the FDTD simulation results of metasurfaces at the focal plane ($z = 14 \mu\text{m}$) corresponding to Figs. 5(d)–5(f). Theoretically, the phase varies in the range of $0 - \pi$ and $0 - 3\pi$ for $l = 0.5$ and 1.5 , and they both have one $0 - \pi$ gap in the phase pattern [circles in Figs. 5(a) and 5(b)], which will generate one intensity gap in the intensity profile of the PV beams [dashed circles in Figs. 5(d), 5(e), 5(g), and 5(h)]. However, we can reorganize the phase distribution to make more $0 - \pi$ gaps and generate more intensity gaps in PV beams [shown in Figs. 5(f) and 5(i)]. The phase profile for generating multiple intensity gaps in Fig. 5(c) can be expressed as²⁹

$$\varphi = \begin{cases} \varphi, & (m-1)\pi < \varphi < (2m-1)\pi \\ \varphi - (2m-1)\pi, & (2m-1)\pi < \varphi < 2m\pi, \\ m = 1, 2, \dots, \text{floor}(l), \end{cases} \quad (6)$$

where $\text{floor}(l)$ means the integer part of topological charge l . The multiple intensity gaps can be used for guiding and transporting particles in optical manipulation application. The simulated generation efficiencies are 75.2%, 74.6%, and 71.0% for elliptical PV beams with $l = 0.5, 1.5$ (single gap), and 1.5 (three gaps).

In conclusion, we have designed and simulated the performance of the all-dielectric silicon metasurfaces and their building blocks. With the help of the selected half-waveplate-like nanoparticles, we can obtain a high-performance metasurface based on the geometrical phase, featuring broadband and high PCE properties in the near infrared range. We designed different metasurfaces for generating PVs with different topological charges l and incident wavelengths, and elliptical PVs with different topological charge l . Moreover, we designed metasurfaces for generating elliptical fraction PVs and studied the effect of the phase gap on the intensity profile. The generation efficiency of the metasurface can reach up to 80% and maintain above 50% at a relatively wide wavelength range (780–880 nm). This work may provide a flexible and compact

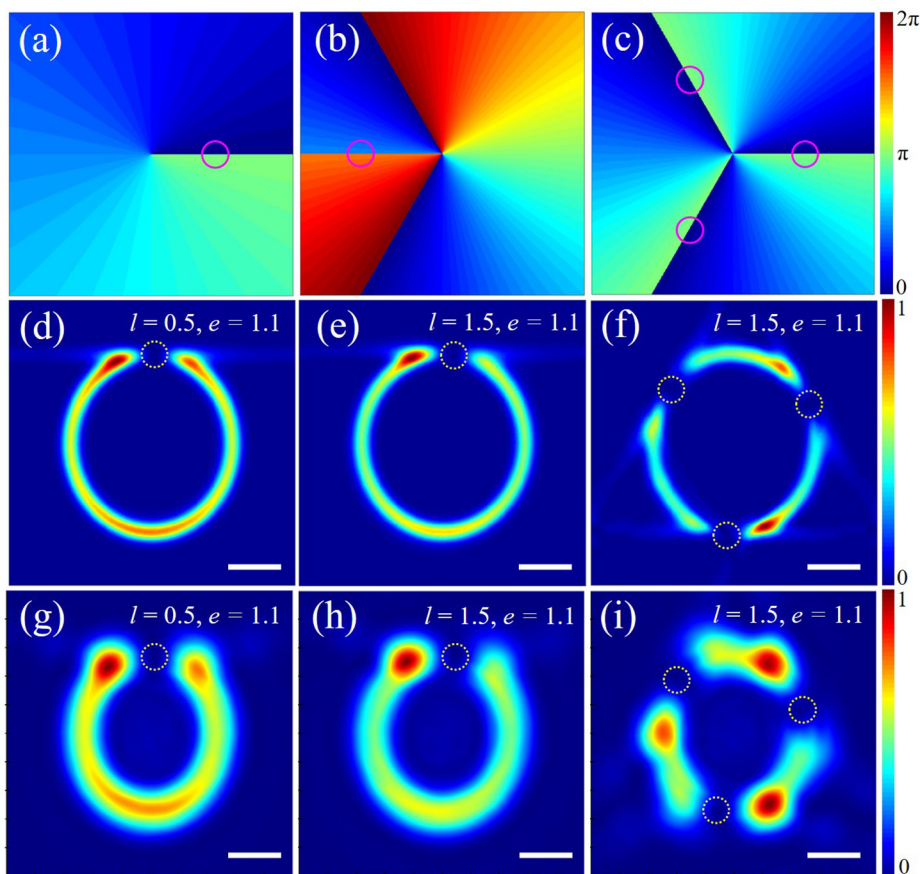


FIG. 5. Theoretical calculated and simulated results of metasurfaces for generating fractional elliptical PV beams with different topological charges. Spiral phase profiles φ_{spiral} with fraction $l=0.5$ in (a), 1.5 in (b) and (c), used for generating fractional PV beams. The circles show the $0-\pi$ gaps in the phase distributions. (d)–(i) Theoretical calculated far-field intensity using the scalar diffraction theory and FDTD simulated intensity at the focal plane corresponding to (a)–(c). The dashed circles show the intensity gaps caused by $0-\pi$ phase shift. Scale bar: $4\ \mu\text{m}$.

platform for optical manipulation, high-resolution microscopy, and on-chip optical communication.

This work was supported by the National Natural Science Foundation of China (No. 11811530052), the Intergovernmental Science and Technology Regular Meeting Exchange Project of Ministry of Science and Technology of China (No. CB02-20), and the Open Fund of State Key Laboratory of Applied Optics (No. SKLAO2020001A04).

AUTHOR DECLARATIONS

Conflict of Interest

The authors declare no conflicts of interest.

DATA AVAILABILITY

The data that support the findings of this study are included within the article.

REFERENCES

- P. Couillet, L. Gil, and F. Rocca, "Optical vortices," *Opt. Commun.* **73**, 403 (1989).
- L. Allen, M. W. Beijersbergen, R. Spreeuw, and J. P. Woerdman, "Orbital angular momentum of light and the transformation of Laguerre-Gaussian laser modes," *Phys. Rev. A* **45**, 8185 (1992).
- J. Wang, J. Y. Yang, I. M. Fazal, N. Ahmed, Y. Yan, H. Huang, Y. X. Ren, Y. Yue, S. Dolinar, M. Tur, and A. E. Willner, "Terabit free-space data transmission employing orbital angular momentum multiplexing," *Nat. Photonics* **6**, 488 (2012).
- M. Padgett and R. Bowman, "Tweezers with a twist," *Nat. Photonics* **5**, 343 (2011).
- A. Nicolas, L. Veissier, L. Giner, E. Giacobino, D. Maxein, and J. Laurat, "A quantum memory for orbital angular momentum photonic qubits," *Nat. Photonics* **8**, 234 (2014).
- A. S. Ostrovsky, C. Rickenstorff-Parrao, and V. Arrizón, "Generation of the "perfect" optical vortex using a liquid-crystal spatial light modulator," *Opt. Lett.* **38**, 534 (2013).
- M. V. Jabir, N. A. Chaitanya, A. Aadhi, and G. K. Samanta, "Generation of "perfect" vortex of variable size and its effect in angular spectrum of the down-converted photons," *Sci. Rep.* **6**, 21877 (2016).
- J. Pinnell, V. Rodríguez-Fajardo, and A. Forbes, "How perfect are perfect vortex beams?," *Opt. Lett.* **44**, 5614 (2019).
- G. Tkachenko, M. Chen, K. Dholakia, and M. Mazilu, "Is it possible to create a perfect fractional vortex beam?," *Optica* **4**, 330 (2017).
- H. T. Chen, A. J. Taylor, and N. Yu, "A review of metasurfaces: Physics and applications," *Rep. Prog. Phys.* **79**, 076401 (2016).
- A. Arbabi, Y. Horie, A. J. Ball, M. Bagheri, and A. Faraon, "Subwavelength-thick lenses with high numerical apertures and large efficiency based on high-contrast transmittarrays," *Nat. Commun.* **6**, 7069 (2015).
- J. Burch, J. Ma, R. I. Hunter, S. A. Schulz, D. A. Robertson, G. M. Smith, J. Wang, and A. D. Falco, "Flexible patches for mm-wave holography," *Appl. Phys. Lett.* **115**, 021104 (2019).
- X. Liu, J. Deng, M. Jin, Y. Tang, X. Zhang, K. F. Li, and G. Li, "Casagrain metasurface for generation of orbital angular momentum of light," *Appl. Phys. Lett.* **115**, 221102 (2019).

- ¹⁴P. Huo, C. Zhang, W. Zhu, M. Liu, S. Zhang, S. Zhang, L. Chen, H. J. Lezec, A. Agrawal, Y. Lu, and T. Xu, "Photonic spin-multiplexing metasurface for switchable spiral phase contrast imaging," *Nano Lett.* **20**, 2791 (2020).
- ¹⁵M. Liu, P. Huo, W. Zhu, C. Zhang, S. Zhang, M. Song, S. Zhang, Q. Zhou, L. Chen, H. J. Lezec, A. Agrawal, Y. Lu, and T. Xu, "Broadband generation of perfect Poincaré beams via dielectric spin-multiplexed metasurface," *Nat. Commun.* **12**, 2230 (2021).
- ¹⁶J. Y. Guo, X. K. Wang, J. W. He, H. Zhao, S. F. Feng, P. Han, J. S. Ye, W. F. Sun, G. H. Situ, and Y. Zhang, "Generation of radial polarized Lorentz beam with single layer metasurface," *Adv. Opt. Mater.* **6**, 1700925 (2018).
- ¹⁷Y. Zhang, W. Liu, G. Jie, and X. Yang, "Generating focused 3D perfect vortex beams by plasmonic metasurfaces," *Adv. Opt. Mater.* **6**, 1701228 (2018).
- ¹⁸J. Han, Y. Intaravanne, A. Ma, R. Wang, S. Li, Z. Li, S. Chen, J. Li, and X. Chen, "Optical metasurfaces for generation and superposition of optical ring vortex beams," *Laser Photonics Rev.* **14**, 2000146 (2020).
- ¹⁹Y. Bao, J. Ni, and C. Qiu, "A minimalist single-layer metasurface for arbitrary and full control of vector vortex beams," *Adv. Mater.* **32**, 1905659 (2020).
- ²⁰Q. Zhou, M. Liu, W. Zhu, L. Chen, Y. Ren, H. J. Lezec, Y. Lu, A. Agrawal, and T. Xu, "Generation of perfect vortex beams by dielectric geometric metasurface for visible light," *Laser Photonics Rev.* **15**, 2100390 (2021).
- ²¹J. Xie, H. Guo, S. Zhuang, and J. Hu, "Polarization-controllable perfect vortex beam by a dielectric metasurface," *Opt. Express* **29**, 3081–3089 (2021).
- ²²J. He, M. Wan, X. Zhang, S. Yuan, L. Zhang, and J. Wang, "Generating ultraviolet perfect vortex beams using a high-efficiency broadband dielectric metasurface," *Opt. Express* **30**, 4806 (2022).
- ²³X. Guo, J. Zhong, P. Li, D. Wen, S. Liu, B. Wei, S. Qi, and J. Zhao, "Metasurface-assisted multidimensional manipulation of a light wave based on spin-decoupled complex amplitude modulation," *Opt. Lett.* **47**, 353 (2022).
- ²⁴H. Zhang, J. Zeng, X. Lu, Z. Wang, C. Zhao, and Y. Cai, "Review on fractional vortex beam," *Nanophotonics* **11**, 241 (2022).
- ²⁵S. H. Tao, X.-C. Yuan, J. Lin, X. Peng, and H. B. Niu, "Fractional optical vortex beam induced rotation of particles," *Opt. Express* **13**, 7726 (2005)..
- ²⁶R. Dasgupta, S. Ahlawat, R. S. Verma, and P. K. Gupta, "Optical orientation and rotation of trapped red blood cells with Laguerre-Gaussian mode," *Opt. Express* **19**, 7680 (2011).
- ²⁷Y. Q. Zhao, X. Zhong, G. H. Ren, S. Y. He, and Z. L. Wu, "Capacity of arbitrary-order orbital angular momentum multiplexing system," *Opt. Commun.* **387**, 432 (2017).
- ²⁸P. Vaity and L. Rusch, "Perfect vortex beam: Fourier transformation of a Bessel beam," *Opt. Lett.* **40**, 597 (2015).
- ²⁹F. Gu, Z. Gu, C. Chang, C. Yuan, S. Feng, F. Xing, and S. Nie, "Generation of tunable fractional vector curvilinear beams with controllable phase distribution," *IEEE Photonics J.* **11**, 6501311 (2019).